

## The Control of Structural and Magnetic Properties in Bismuth Substituted Cobalt Ferrite by Heat Treatment

Retna Arilasita<sup>1</sup>, Suharno<sup>2\*</sup>, Utari<sup>1</sup>, Budi Purnama<sup>1\*</sup>

<sup>1</sup>Department of Physics, Faculty of Mathematics and Natural Sciences  
Universitas Sebelas Maret, Surakarta 57126, Indonesia

<sup>2</sup>Department of Physics Education, Faculty of Teacher Training and Education,  
Universitas Sebelas Maret, Surakarta 57126, Indonesia

Received 22 April 2021, Revised 8 June 2021, Accepted 13 June 2021

### ABSTRACT

*The bismuth substituted cobalt ferrite  $\text{CoBi}_x\text{Fe}_{2-x}\text{O}_4$  ( $x = 0.1$ ) were synthesized by co-precipitation procedure. The properties of the samples were controlled by heat treatment through annealing processes at temperatures of 300 °C, 400 °C, and 500 °C. After that, all samples were characterized by XRD, FTIR, and VSM. The high purity fcc inverse spinel with  $Fd-3$  space group is obtained following the Rietveld refinement of XRD. The spectrum analysis in the range 400-600  $\text{cm}^{-1}$  confirms the spinel ferrite structure. The net magnetic moment  $n_B$ , coercive field  $H_C$ , and magnetization saturation  $M_S$  of the co-precipitated bismuth substituted cobalt ferrite samples increase with increasing annealing temperature which attributes to the increase of the anisotropy constant.*

Keywords: nanoparticles, bismuth cobalt ferrite, annealing, co-precipitation, cubic

### 1. INTRODUCTION

Cobalt ferrite present in the spinel oxide has a face-centered cubic structure. The cobalt ferrite nanoparticles have advantages such as high coercivity values, medium saturation magnetization values and good mechanical properties, hence their preference [1]. Previous work have explained that the physical and chemical properties of cobalt ferrite can be controlled by ionic substitution [2-6], synthesis methods [7-11], thermal treatment [12,13] and others. Recently, researchers have focused on bismuth-doped cobalt ferrite as they determine the distorted structure in the sample. The bismuth-doped cobalt ferrite has been investigated and they have prepared the sample successfully by auto combustion technique. Because of bismuth doping, they found an increase in particle size. This could consistently change its electrical properties of the material in the form of increased resistivity, grain size evolution and minimizes dielectric loss and a good conduction material [14]. An investigation of sol-gel combustion and co-precipitation method of bismuth substituted cobalt ferrite was also reported. The crystallite size with the co-precipitation method was found to be much smaller than the sol-gel combustion method, while the magnetic properties were almost the same [15]. They found that the coercive field of bismuth cobalt ferrite greater than pure cobalt ferrite [16].

---

\*Corresponding author: bournama@mipa.uns.ac.id; suharno\_71@staff.uns.ac.id

Other researchers also found that the crystal structure, electrical, and magnetic parameters of the sample could be modified by replacement of  $\text{Bi}^{3+}$  ions in  $\text{Fe}^{3+}$  ions [17-19].

The heat annealing treatment can easily modify the crystallite size of the particles and the coercivity value. It is known that the coercivity value increases with thermal treatment, this was possibly induced by a stronger exchange interaction as organic degradation in thermal [20]. When the nanoparticles were heated, there was the energy that allows the cation to diffuse and produce a balanced state. At high temperatures, the distribution site can be maintained after cooling to room temperature [21]. The heat energy from the calcination temperature was used by the nanoparticles to diffuse to form larger granular particles and larger distribution [22].

In this study, the bismuth-doped cobalt ferrite was synthesized by the co-precipitation technique. To modify the properties of the nanoparticles, a heat annealing treatment will be carried out at different temperatures. The results of bismuth substituted cobalt ferrite were characterized using x-ray diffraction (XRD), fourier transforms infrared (FTIR), and vibrating sample magnetometer (VSM).

## 2. MATERIAL AND METHODS

The materials with chemical composition of  $\text{Fe}(\text{NO}_3)_3 \cdot 9\text{H}_2\text{O}$ ,  $\text{Co}(\text{NO}_3)_2 \cdot 6\text{H}_2\text{O}$ , and  $\text{Bi}(\text{NO}_3)_3 \cdot 5\text{H}_2\text{O}$  were used to synthesize  $\text{CoBi}_x\text{Fe}_{2-x}\text{O}_4$  (%wt,  $x = 0.1$ ) by co-precipitation technique. Double distilled water was used to dissolve a weighted stoichiometric amount of metal salt which is then stirred continuously over the magnetic hotplate for 20 minutes. The solution was heated under continuous stirring (low stirring at 250 rpm). The concentration of 4.8 M NaOH solution was added to the metal salt solution mixture and the reaction mixture temperature was maintained at  $85^\circ\text{C}$ . After that, the solution was left to sit overnight to form a precipitate, then washed using ethanol and distilled water. The precipitate was dried in an oven at  $100^\circ\text{C}$  overnight. The dry precipitate was hand-milled with a mortar for 1 hour to obtain a powder sample. Finally, at the final stage, the powder was annealed at different temperatures ( $300^\circ\text{C}$ ,  $400^\circ\text{C}$ , and  $500^\circ\text{C}$ ) for 5 hours and then hand-milled again for 2 hours to obtain the final product.

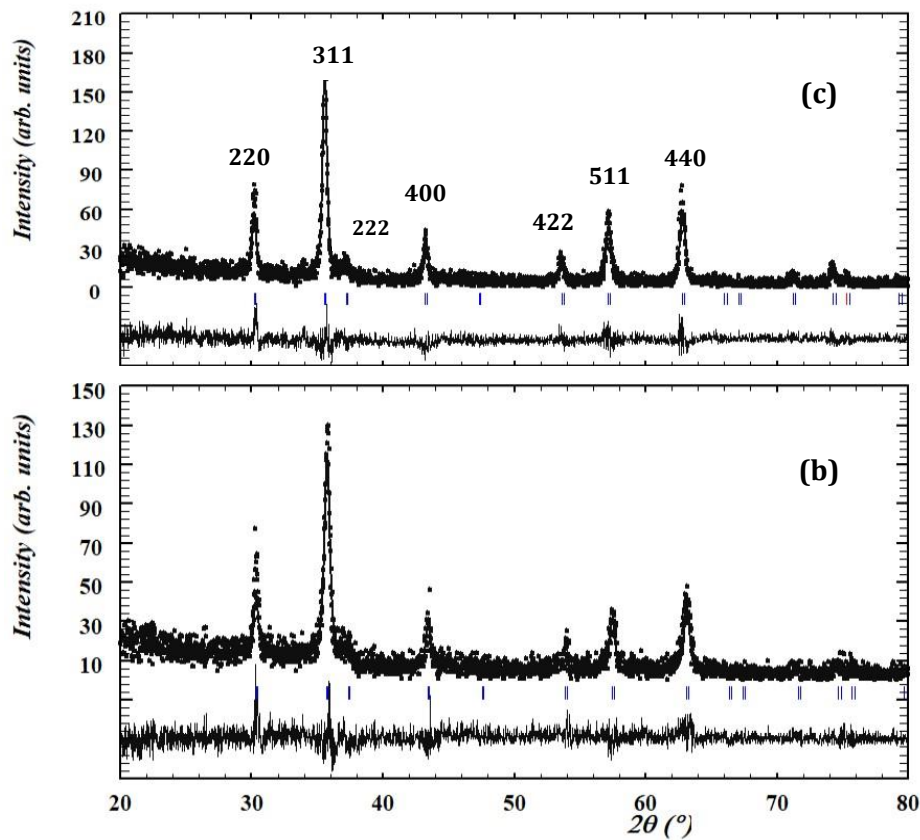
The structural properties of the samples were determined by qualitative x-ray powder diffraction measurements using the XRD (using  $\text{Cu-K}\alpha$  radiation,  $\lambda = 1.54 \text{ \AA}$ ) at room temperature. The XRD patterns of the samples were recorded in the range  $2\theta = 20-90^\circ$ . The oxide bonds were determined by FTIR-Shimadzu IF Prestige 21 spectroscopy and IR spectra were recorded in the range  $350 - 4000 \text{ cm}^{-1}$ . The VSM at room temperature was used for magnetic measurements.

## 3. RESULTS AND DISCUSSION

### 3.1 The Structural

The X-ray diffraction patterns were analyzed with the Fullprof program using the Rietveld technique. The diffraction pattern of XRD measurements showed the bismuth substituted cobalt ferrite structure with the  $\text{Fd-3m}$  space group. The XRD patterns with refine data are shown in Figure 1. Figure 1 shows a diffraction pattern with a Miller Indices  $hkl$  peak (220), (311), (222), (400), (422), (511), and (440) where the peaks were a cobalt ferrite phase with a cubic crystal system and space group  $\text{Fd-3m}$ . The XRD patterns in all samples show a single phase. The Scherrer equation was used to calculate the crystal size. The crystal sizes were found to be 15.65 nm, 18.83 nm, and 20.35 nm for each annealing temperature of  $300^\circ\text{C}$ ,  $400^\circ\text{C}$ , and  $500^\circ\text{C}$ . The crystal size of cobalt ferrite-based

materials have the potential to influence magnetic properties. The crystal structure analysis also explains that the difference in annealing temperatures at 300°C, 400°C, and 500°C will affect the shift of the diffraction pattern peaks. In the refining process, the position of the oxygen atom has been taken as a changeable parameter. Meanwhile, the position of the other atoms was fixed. The positions of the Co, Fe and O atoms from the refined results with foolproof were as shown in Table 1. The position of the oxygen atom changes due to the annealing treatment. The background has been corrected by the pseudo-Voigt function. The Rietveld refinement parameters of all samples were given in Table 2. The various R factors such as  $R_p$  (profile factor),  $R_F$  (crystallographic factor), and  $R_B$  (Bragg factor) were found to decrease with increasing annealing. The  $R_p$  value obtained is quite large due to the high ratio of the diffraction pattern calculation and experimental XRD measurement results for the nanocrystalline material [23]. However, the value of  $\chi^2$  (goodness of fit) was observed to be of small value which indicates the goodness of refinement. The lattice parameter  $a$  and unit cell volume  $V$  were slightly increased with annealing treatment. It is indicated that the original structure of bismuth substituted cobalt ferrite remains with the increase in annealing.



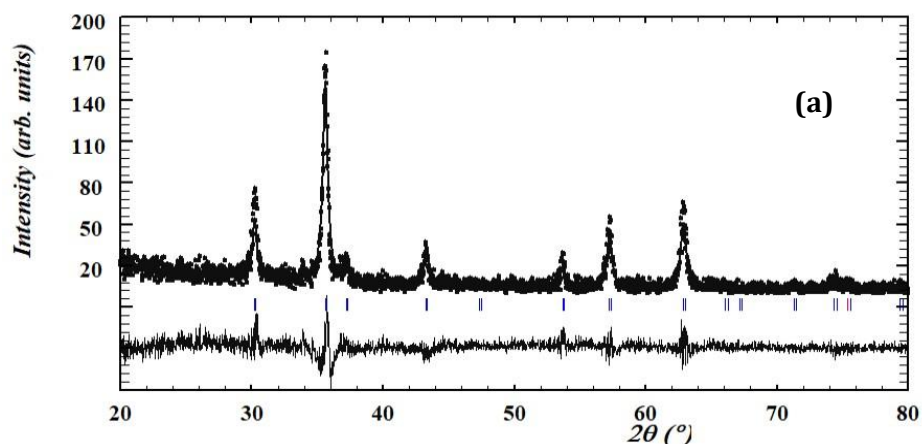


**Figure 1** The refine data of XRD patterns for  $\text{CoBi}_x\text{Fe}_{2-x}\text{O}_4$  ( $x = 0.1$ ) annealed at (a) 300°C, (b) 400°C and (c) 500°C

**Table 1** The atomic positions ( $x,y,z$ ) of Co, Fe, and O for  $\text{CoBi}_x\text{Fe}_{2-x}\text{O}_4$  (%wt,  $x = 0.1$ ) at various annealing temperature

Atomic positions	Annealing temperature (°C)		
	300	400	500
<b>Co/Fe,Bi</b>			
x	0.12500	0.12500	0.12500
y	0.12500	0.12500	0.12500
z	0.12500	0.12500	0.12500
<b>Fe, Bi/Co</b>			
x	0.50000	0.50000	0.50000
y	0.50000	0.50000	0.50000
z	0.50000	0.50000	0.50000
<b>O</b>			
x	0.26037	0.26007	0.25664
y	0.26037	0.26007	0.25664
z	0.26037	0.26007	0.25664

**Table 2** The refine data for  $\text{CoBi}_x\text{Fe}_{2-x}\text{O}_4$  (%wt,  $x = 0.1$ ) at various annealing temperature

Structural parameters	Annealing temperature (°C)		
	300	400	500
<b>Crystal System</b>	Cubic	Cubic	Cubic
<b>Number of space group</b>	227	227	227
<b>Space group</b>	Fd-3m	Fd-3m	Fd-3m
<b><math>R_p</math> (%)</b>	50.18	40.42	30.60
<b><math>R_F</math> (%)</b>	13.79	8.73	6.89
<b><math>R_B</math> (%)</b>	15.54	10.73	8.39
<b><math>\chi^2</math></b>	2.05	1.95	1.88
<b><math>a = b = c</math> (Å)</b>	8.3294	8.3589	8.36750
<b><math>\alpha = \beta = \gamma</math></b>	90	90	90
<b><math>V</math> (Å<sup>3</sup>)</b>	577.8746	584.0453	585.853

### 3.2 The FTIR Study

The FTIR spectra of bismuth-doped cobalt ferrite at different annealing temperatures were shown in Figure 2. The first characteristic absorption of the three samples appears around  $\sim 3450\text{ cm}^{-1}$  which was thought to be due to the hydrogen bond O-H stretching mode [24]. Meanwhile, the absorption band around  $\sim 1682\text{ cm}^{-1}$  was considered to originate from the C=O stretching vibration [25]. Then the peak of the absorption band around  $\sim 1350\text{ cm}^{-1}$  establishes the O-H bending of all samples. Two main bands were detected around wave number  $400\text{-}600\text{ cm}^{-1}$  in all samples. The absorbance peak of  $\nu_1$  shows the high-frequency band (around  $600\text{ cm}^{-1}$ ) which related to the stretching vibration of the iron-oxygen bond (Fe-O) at the tetrahedral site, whereas  $\nu_2$  shows the low-frequency band (around  $400\text{ cm}^{-1}$ ) which related to the stretching vibration of the cobalt-oxygen bond (Co-O) at the octahedral site [26]. The range of vibration bands corresponds to the spinel phase of the ferrite [27]. These results confirmed the emergence of cobalt ferrite synthesized by the co-precipitation techniques. Increasing the annealing temperature causes the position of the  $\nu_1$  and  $\nu_2$  bands to shift to a lower wavenumber. It is indicated that cation redistribution at tetrahedral and octahedral are due to annealing temperature.

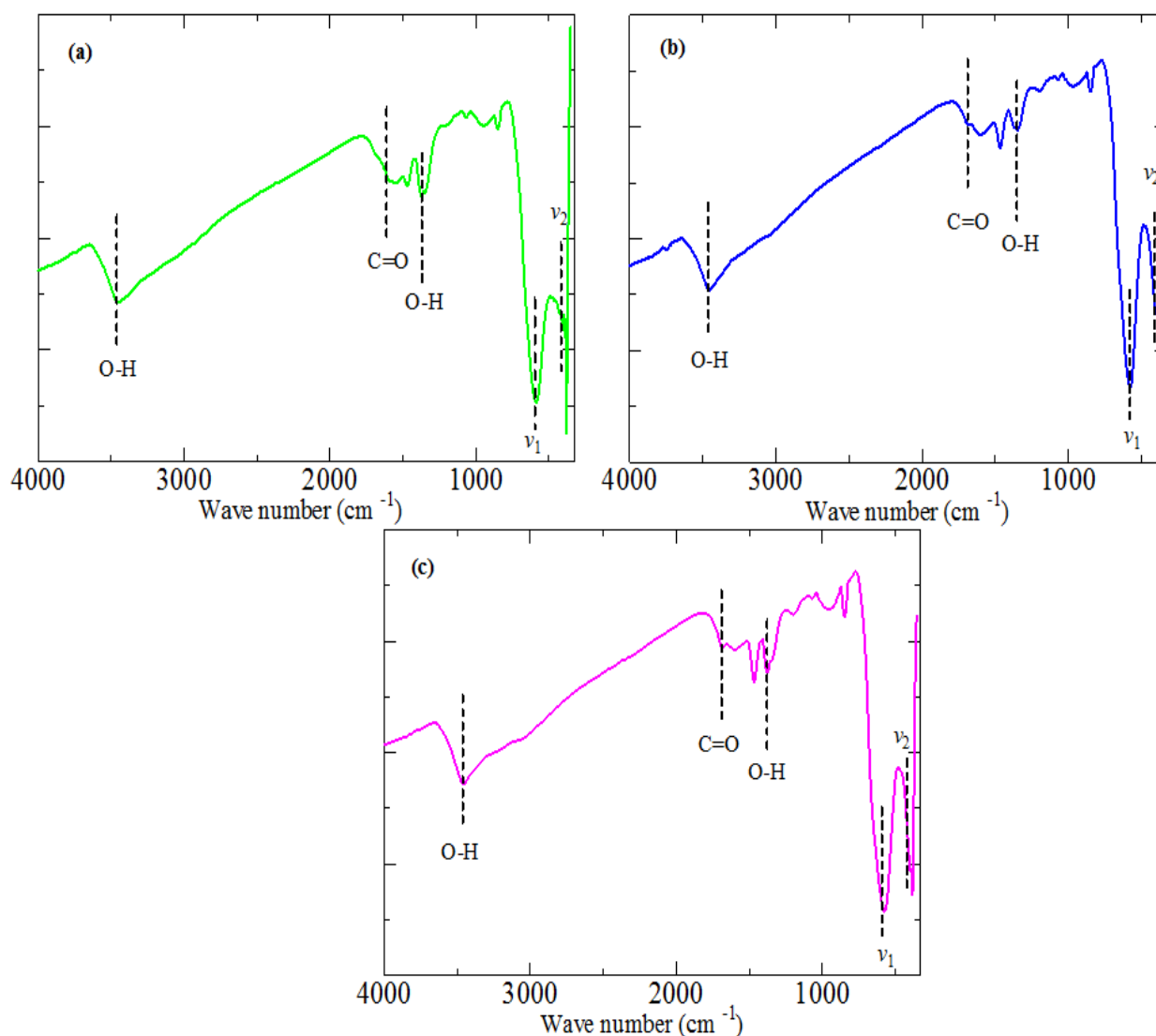


**Figure 2** The infrared spectra of  $\text{CoBi}_x\text{Fe}_{2-x}\text{O}_4$  (%wt,  $x = 0.1$ ) with (a)  $T_A = 300^\circ\text{C}$ , (b)  $T_A = 400^\circ\text{C}$ , (c)  $T_A = 500^\circ\text{C}$

### 3.3 The Magnetic Properties

The magnetic hysteresis loop of bismuth substituted cobalt ferrite nanoparticles with different annealing temperatures are shown in Figure 3. The magnetic parameters such kind magnetization saturation  $M_S$  and coercive field  $H_C$  obtained were shown in Table 3. The magnetization saturation  $M_S$  and coercive field  $H_C$  increase with the increase of annealing temperature which presents in Figure 4, i.e., the  $H_C$  and the  $M_S$  (inset) as a function of annealing temperature. Here, the calculation of the  $H_C$  is 330.23, 423.42, and 588.32 Oe, for the annealing temperature of  $300^\circ\text{C}$ ,  $400^\circ\text{C}$ , and  $500^\circ\text{C}$ . Whereas, the  $M_S$  is 25.07, 423.42, and 588.32 emu/g as within the increase of annealing temperature. Here, the  $H_C$  and the  $M_S$  increase with the increase of annealing temperature. The ratio squareness ( $M_r/M_S$ ) is 0.29, 0.33 and 0.41, for annealing temperatures of  $300^\circ\text{C}$ ,  $400^\circ\text{C}$ , and  $500^\circ\text{C}$  respectively. As discussed in the previous section, the degree of conformity of the x-ray diffraction pattern

increases with increasing annealing temperature in the rietveld calculation results. This indicates that the increase in annealing temperature increases the magnetic anisotropy of this bismuth substituted cobalt ferrite sample. In order to confirm these experimental results, the net moment magnetic as well as magnetic-anisotropy constant calculations were carried out concerning the annealing temperature increase.

The net magnetic moment  $n_B$  [28] in Bohr magneton ( $\mu_B$ ) was calculated using the following equation (1):

$$n_B = \frac{M \times M_s}{N_A \times 9.27 \times 10^{-21}} \quad (1)$$

where  $M$  is the molecular weight,  $M_s$  is the saturation magnetization of the sample, and  $N_A$  is Avogadro's number. It is clear that  $n_B$  corresponds to  $M_s$ , where the trend shows an increase with the annealing temperature. The  $n_B$  of 1.12, 1.73, and 1.83 are obtained for annealing temperatures of 300°C, 400°C, and 500°C, respectively. Whereas the anisotropy constant  $K$  is calculated using the equation (2) [29]:

$$H_C = \frac{0.96K}{M_s} \quad (2)$$

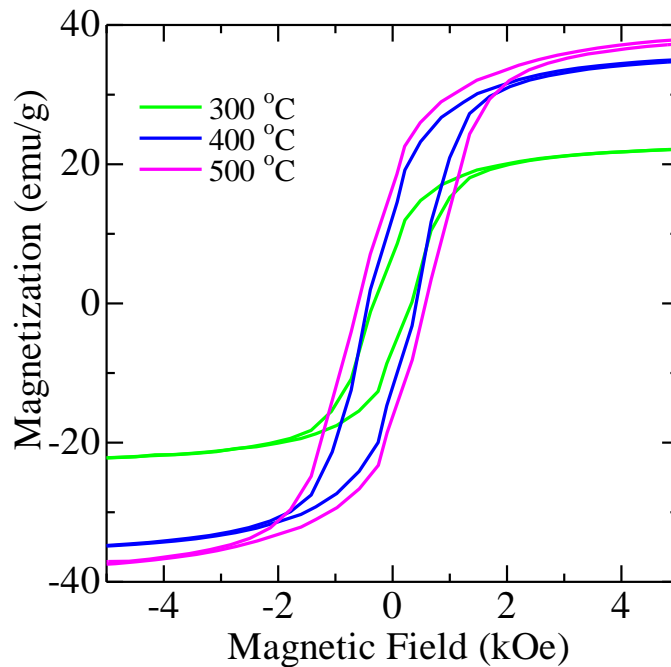


**Figure 3** The loop M-H of  $\text{CoBi}_x\text{Fe}_{2-x}\text{O}_4$  (%wt,  $x = 0.1$ ) with annealing temperature variation of 300°C, 400°C, and 500°C

The anisotropy constant  $K$  is obtained  $0.49 \times 10^5$  (erg/cm<sup>3</sup>) for an annealing temperature of 300°C. Thus, the  $K$  of  $0.97 \times 10^5$  (erg/cm<sup>3</sup>) and  $1.41 \times 10^5$  (erg/cm<sup>3</sup>) with annealing temperature of 400°C and 500°C. The results of the calculation of the  $K$  confirm that the increase in annealing temperature

increases the  $K$ . As a result, the magnitude of the coercive field  $H_c$  and saturation magnetization increases  $M_s$  with increasing annealing temperature.

**Table 3** The magnetic properties of  $\text{CoBi}_x\text{Fe}_{2-x}\text{O}_4$  (%wt,  $x = 0.1$ ) with annealing temperature variation of  $300^\circ\text{C}$ ,  $400^\circ\text{C}$ , and  $500^\circ\text{C}$

$T_a$ ( $^\circ\text{C}$ )	$H_c$ (Oe)	$M_s$ (emu/g)	$M_r$ (emu/g)	$M_r/M_s$	$n_B$ ( $\mu_B$ )	$K \times 10^5$ (erg/cm $^3$ )
300	330.23	25.07	7.36	0.29	1.12	0.49
400	423.42	38.81	12.87	0.33	1.73	0.97
500	588.32	41.00	16.92	0.41	1.83	1.41

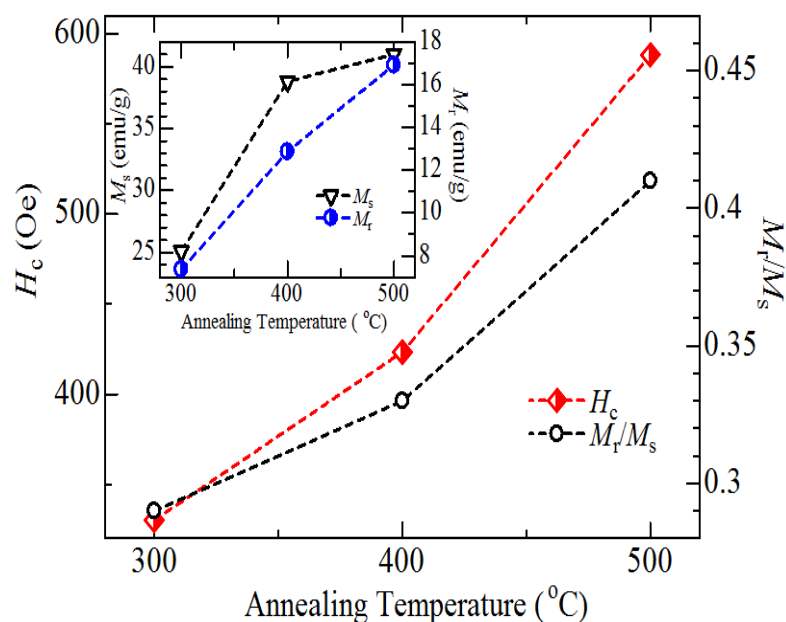


**Figure 4** The relationship between annealing temperature and magnetic parameters of  $\text{CoBi}_x\text{Fe}_{2-x}\text{O}_4$  (%wt,  $x = 0.1$ )

#### 4. CONCLUSION

The bismuth-doped cobalt ferrite has been successfully synthesized using a co-precipitation procedure with the variation of the heat treatment. The Rietveld refinement of the XRD pattern used to evaluate the x-ray pattern shows that the high purity fcc inverse spinel with  $Fd-3m$  space group. The FTIR data also indicate the spinel ferrite structure. The net magnetic moment  $n_B$ , coercive field  $H_c$ , and magnetization saturation  $M_s$  of the coprecipitated bismuth substituted cobalt ferrite samples increase with the increase of the annealing temperature. The calculation of the magnetic anisotropy constant confirmed the increase with the annealing temperature which contributed to changes in the whole magnetic parameters of the obtained sample.

## ACKNOWLEDGMENTS

This research was funded by Penelitian Unggulan Terapan, DIPA Non APBN Universitas Sebelas Maret, Kementerian Pendidikan dan Kebudayaan, RI at contract No.260/UN27.22/HK.07.00/2021.

## REFERENCES

- [1] Rachna, Singh NB, Agarwal A., "Preparation, Characterization, Properties, and Applications of nano Zinc Ferrite," *Materials Today: Proceedings*. Elsevier BV, vol **5**, issue 3 (2018) pp. 9148–9155.
- [2] R. Jabbar, S. H. Sabeeh, and A. M. Hameed, *J. Magn. Magn. Mater.* vol **494**, (2020), p.165726.
- [3] P. Imanipour, S. Hasani, M. Afshari, S. Sheykh, A. Seifoddini, and K. Jahanbani-Ardakani, *J. Magn. Magn. Mater.* vol **510**, (2020) p. 166941.
- [4] M. Kamran and M. Anis-ur-Rehman, *J. Alloys Compd.* vol **822**, (2020) p. 153583.
- [5] Furtado NJS, Magalhães J.L., *Journal of Electroanalytical Chemistry*. Elsevier BV, vol **871**, (2020) p. 114315.
- [6] M. I. A. A. Maksoud, G. S. El-Sayyad, A. H. Ashour, A. I. El-Batal, M. S. Abd-Elmonem, H. A. Hendawy, M. M. El-Okr, *Mater. Sci. Eng. C*. vol **92**, (2018) pp. 644-656.
- [7] Zalite I, Heidemane G, Kuznetsova L, Kodols M, Grabis J, Maiorov M., *Chemical Technology Publishing House Technologija*, vol **67**, issue 1 (2016).
- [8] J. Venturini, A. M. Tonelli, T. B. Wermuth, R. Y. S. Zampiva, S. Arcaro, A. D. C. Viegas, & C. P. Bergmann, *J. Magn. Magn. Mater.* vol **482**, (2019) pp. 1-8.
- [9] A. Maleki, N. Hosseini, and A. R. Taherizadeh, *Ceram. Int.* vol **44**, issue 7 (2018) pp. 8576-8581.
- [10] Kumari C, Lahiri P., "Synthesis and Characterization of Nickel-Based Cobalt Ferrite Nanopowder", *Macromolecular Symposia*. Wiley, vol **388**, issue 1 (2019) p. 1900026.
- [12] E. Hutamaningtyas, Utari, Suharyana, B. Purnama, and A. T. Wijayanta, *J. Korean Phys. Soc.* **69**, issue 4 (2016) pp. 584-588.
- [13] R. Arilasita, Utari, and B. Purnama, *J. Korean Phys. Soc.* vol **74**, issue 5 (2019) pp. 498-501.
- [14] Franco A, Pessonni HVS, Alves TEP., *Materials Letters*. Elsevier BV, vol **208** (2017) pp. 115–117.
- [15] V. S. Kiran and S. Sumathi, *J. Magn. Magn. Mater.* vol **421**, (2017) pp. 113-119.
- [16] D. E. Saputro, U. Utari, and B. Purnama, *J. Phys. Theor. Appl.* vol **3**, issue 1 (2019) p. 9
- [17] K. Vijaya Kumar and N. Suresh Kumar, *Mater. Today Proc.*, vol **3**, issue 10 (2016) pp. 4193-4198.
- [18] Imanipour P, Hasani S, Seifoddini A, Farnia A, Karimabadi F, Jahanbani-Ardakani K, *Journal of Sol-Gel Science and Technology*. Springer Science and Business Media LLC, vol **95**, issue 1 (2020) pp. 157–167.
- [19] K. L. Routray, D. Sanyal, and D. Behera, *J. Appl. Phys.* vol **122**, issue 22 (2017) p. 224104.
- [20] Lartigue L, Innocenti C, Larionova J, Guari Y., *Journal of Nanoscience and Nanotechnology*. American Scientific Publishers, vol **19**, issue 8 (2019) pp. 5000–5007.
- [21] E. H. El-Ghazzawy, *J. Magn. Magn. Mater.* vol **497**, (2020) p. 166017.
- [22] B. Purnama, A. T. Wijayanta, and Suharyana, *J. King Saud Univ.-Sci.* vol **31**, issue 4 (2019) pp. 956-960.
- [23] R. Kumar and M. Kar, *J. Magn. Magn. Mater.* vol **416**, (2016) pp. 335-341.
- [24] A. Samavati, M. K. Mustafa, A. F. Ismail, and M. H. D. Othman, *Mater. Exp.* vol **6**, issue 6 (2016) pp. 473-482.
- [25] N. Adeela, U. Khan, S. Naz, K. Khan, R. U. R. Sagar, S. Aslam, & D. Wu, *Mater. Res. Bull.*, vol **107**, (2018) pp. 60-65.
- [26] Chitra C, Raguram T, Rajni K.S., *International Journal of Trend in Scientific Research and Development*. South Asia Management Association, vol **2**, issue 5 (2018) pp. 371-377.

- [27] B. Purnama, R. Rahmawati, A. T. Wijayanta, and Suharyana, *J. Magn.* vol **20**, (2015) pp. 207-210.
- [28] S. Nasrin, F. U. Z. Chowdhury, and S. M. Hoque, *J. Magn. Magn. Mater.* vol **479**, (2019) pp. 126-134.
- [29] E. H. El-Ghazzawy & M. A. Amer, *J. Alloys Compd.* vol **690**, (2017) pp. 293-303.